Am J Cancer Res 2019;9(3):529-545
www.ajcr.us /ISSN:2156-6976/ajcr0090406

Original Article

Respiratory hyperoxia reverses immunosuppression by regulating myeloid-derived suppressor cells and PD-L1 expression in a triple-negative breast cancer mouse model

Xueke Qian[1], Qi Zhang[1], Nan Shao[1], Zhen Shan[1], Tuckyun Cheang[1], Zhanqiang Zhang[1], Qiao Su[2], Shenming Wang[1*], Ying Lin[1*]

[1]Department of Thyroid and Breast Surgery, [2]Animal Experiment Center, The First Affiliated Hospital of Sun Yat-sen University, NO. 58 Zhongshan Road 2, Guangzhou 510080, China. [*]Equal contributors.

Received December 25, 2018; Accepted February 1, 2019; Epub March 1, 2019; Published March 15, 2019

Abstract: Hypoxia plays an extensive role in the development of the tumor microenvironment (TME), particularly in mediating immunosuppression. Respiratory hyperoxia therapy has the potential to improve the effects of conventional cancer therapies via molecular mechanisms mediating antitumor immunity. Here, we investigated whether hyperoxia therapy can restore tumor immunity and inhibit lung metastases in a mouse model of triple-negative breast cancer (TNBC) by treating a 4T1 mammary carcinoma mouse model with normoxia (21% oxygen) or hyperoxia (60% oxygen) therapy, after tumor development. Using flow cytometry analysis, we observed significant organ-specific expansion of myeloid-derived suppressor cells (MDSCs) and protein expression upregulation of the programmed death-ligand 1 (PD-L1) in the hypoxic TME of 4T1 tumor-bearing mice maintained under normoxia conditions, with the TME converting to a T-cell immune-suppressive state as early as the premetastatic phase. Markedly, hyperoxia treatments ameliorated hypoxia levels in the lung TME and decreased the proportion of MDSCs and the expression of PD-L1 in both the primary tumor and in the metastatic lung, when compared to animals treated with respiratory normoxia therapy. In addition, the number of lung metastatic nodes fell from 90 per lung in the normoxic treated group to 13 per lung in the hyperoxic treated group ($P < 0.05$), with the latter having limited hyperoxia effects on primary tumor growth (mammary glands). Notably, hyperoxia therapy was characterized by the differential recruitment of $CD4^+$ and $CD8^+$ T-cells. Thus, our study confirms that hyperoxia therapy may be used to overcome TME immunosuppression and control the extend of lung metastases in TNBC. Importantly, changes in immunosuppressive MDSCs frequency and PD-L1 expression levels may serve as biomarkers of hypoxia levels in cancer affected tissues that can benefit from hyperoxia treatments.

Keywords: Respiratory hyperoxia therapy, hypoxia, tumor microenvironment, programmed death-ligand 1, myeloid-derived suppressor cells, lung metastasis, 4T1 mammary carcinoma, tumor immunity, T-cell immune-suppression

Introduction

The degree of hypoxia in the tumor microenvironment (TME) is considered one of the most significant determinants of cancer progression [1-3]. Among all the effects mediated by hypoxia, an important one is the ability to regulate immunosuppressive mechanisms that involve myeloid-derived suppressor cells (MDSCs), tumor-associated macrophages (TAMs), regulatory T-cells (Treg cells), and immune checkpoint pathways, such as the programmed cell death-1 (PD-1)/programmed death-ligand 1 (PD-L1) [4-6]. Hypoxia induces the recruitment of MDSCs to the primary tumor and regulates the function and differentiation of MDSCs in the TME [4, 7]. Importantly, hypoxia induces PD-L1 expression via transcription factor activation, such as the hypoxia-inducible factor 1 (HIF-1), which is present in cells belonging to the TME [8]. Notably, both, MDSCs and PD-L1 signals are major components of the immune-suppressive TME [9, 10].

Given the role of hypoxia in regulating immunosuppression, significant attention is being paid

to the potential of respiratory hyperoxia therapy in restoring tumor immunity and in treating cancer progression [11, 12]. Currently, respiratory hyperoxia is mainly used for the treatment of hypoxic tissue damage, however it has also been shown to improve oxygen supply to hypoxic tumor zones in animal models [13]. In addition, respiratory hyperoxia has been shown to improve the treatment efficacy of chemotherapeutic agents and drug resistance in rat mammary tumors and osteosarcoma mouse models [14, 15]. Clinical studies in early development have shown that respiratory hyperoxia can effectively treat malignant gliomas, when used in combination with radiotherapy and chemotherapy modalities [16, 17]. Therefore, it is likely that the molecular mechanisms underlying the benefits of hyperoxia therapy are related to tumor immunity. Notably, a previous study reported that respiratory hyperoxia served as an immunological adjuvant therapy combined with dual immunotherapy treatments, in the form of monoclonal antibodies [mAbs] for CTLA-4/PD-1 immunocheckpoint pathways in metastatic tumors [11]. Respiratory hyperoxia has been also shown to inhibit immunosuppressive pathways, such as the CD39/CD73-A2AR/A2BR in the TME [12].

Triple-negative breast cancer (TNBC) is a highly immunogenic type of breast cancer with a poor prognosis that is associated with a high risk of distant metastasis [18]. Importantly, the lungs are common target sites for TNBC metastases [19]. Therefore, immunotherapeutic strategies, which intend to trigger or enhance antitumor immunity are attractive treatment options for the clinical management of metastases in TNBC patients [20]. Recent studies have shown that immune suppression reversal could inhibit metastases in a TNBC mouse model [21]. In addition, clinical trials have shown that monoclonal antibodies blocking the PD-1/PD-L1 pathway play a therapeutic role in metastatic TNBC patients [22]. Another clinical trial reported a significant high response rate in metastatic TNBC patients treated with both a PD-L1 inhibitor (atezolizumab) and the nanoparticle albumin-bound chemotherapeutic agent, paclitaxel (nab-paclitaxel) [23].

Given the status of the current research, we sought to investigate whether hyperoxia therapy could prevent and/or regulate immunosuppression of the lung TME in metastatic TNBC and evaluated the underlying molecular mechanisms driving this regulation. To this end, a 4T1 mammary carcinoma mouse model was developed for this study, given that the 4T1 mammary carcinoma transplantable tumor cell line can spontaneously metastasize throughout the body, thereby mimicking TNBC in humans. Moreover, it has been reported that 4T1 tumor mouse models can be effectively treated via the elimination of MDSCs [21, 24]. In our study, hyperoxia (60% oxygen) was selected for our respiratory treatment, given the fact that this is a concentration considered clinically safe in humans in other indications [25]. Here, we demonstrate that respiratory hyperoxia treatment reduces hypoxia in the lungs of the metastatic 4T1 TNBC mouse model. Particularly, reduced hypoxia inhibits the recruitment of bone marrow (BM) MDSCs to metastatic tumors in the lungs, in addition to primary tumors of the mammary glands. Reduced hypoxic conditions in the TME can lead to decreased PD-L1 expression levels, which in turn, promote the regression of the primary tumor and lung metastases by promoting tumor immunity in the TME.

Overall, respiratory hyperoxia therapy appears to effectively overcome immunosuppression in the TME, limiting lung metastases in a TNBC mouse model. For TNBC patients, respiratory hyperoxia therapy may be a valuable modality for antitumor treatment. Moreover, the frequency of MDSCs and levels of PD-L1 expression might also serve as biomarkers of hypoxia and hyperoxia treatment efficacy.

Cell lines and mice

4T1 mammary carcinoma cells were obtained from the American Type Culture Collection (ATCC; Manassas, VA, USA), and were cultured in RPMI-1640 media, supplemented with 10% (v/v) fetal bovine serum (FBS, Gibco-Invitrogen; Waltham, MA, USA), 100 U/mL penicillin, and 100 μg/mL streptomycin (all from Gibco-Invitrogen) at 37°C, in a 5% CO_2 humidified incubator. 8-12 weeks old wild-type BALB/c female mice, were purchased from Vital River Laboratory Animal Technology Co., Ltd. (Beijing, China) and bred in our animal facility under specific-pathogen-free conditions. All animal procedures were performed under protocols that complied with the Institutional Animal Care and Use Committee Guidelines for Ethical Conduct in the Care and Use of Animals.

4T1 TNBC mouse model

Approximately 10^5 4T1 cells suspended in 50 µl of Hank's Balanced Salt Solution (HBSS, Gibco-Invitrogen) were injected subcutaneously (sc) into the fourth abdominal mammary gland of BALB/c female mice. The appearance of tumors was monitored daily by palpating the injection area with gloved fingers, which happened approximately between day 5 and day 7, with all tumors being palpable by day 7 (Figure S1A). When a tumor was palpable, the primary tumor diameter (TD) was measured every two days using vernier calipers. The tumor volume was then calculated according to the formula: $V = (a^2 \times b)/2$, where 'a' is the shortest transverse diameter and 'b' is the longest transverse diameter. Experimental mice were sacrificed when the TD reached 14 to 16 mm or the mice became moribund (according to the University of Maryland Baltimore County Institutional Animal Care and Use Committee guidelines), occurring approximately between day 28 to day 35 (Figure S1B). On day 0, 7, 14, 21, or 28, tissues of interest from tumor-bearing mice and tumor-free mice were harvested and fixed in 10% paraformaldehyde (PFA) for hematoxylin and eosin stain (H&E) stain and immunofluorescence analysis (IF) or were processed immediately using flow cytometric imaging techniques.

Clonogenic assays for the evaluation of spontaneous lung metastases

The clonogenic procedure used in this study has been described previously [26] and was performed with minor modifications. In brief, on day 7, 14, or 21, 4T1 tumor-bearing mice were sacrificed, and their lungs were harvested. Lung samples were finely minced and digested in 5 ml of an enzyme cocktail containing 1 × RPMI-1640, 2% (v/v) FBS, 0.002% (w/v) collagenase D (Sigma-Aldrich; Saint Louis, MO, USA) and 0.002% (w/v) DNA polymerase I (Sigma-Aldrich) for 1 hour at 37°C. All samples were then filtered through a 70 µm cell strainer (BD Biosciences; San Jose, CA, USA) and washed twice with 1 × phosphate buffered saline (PBS; Gibco-Invitrogen). Single-cell suspensions from the lungs of each mouse were plated into a 10 cm tissue culture dish in medium containing 60 mM of 6-thioguanine (Sigma-Aldrich) to selectively grow tumor cells. After 10 to 14 days, the cells were fixed in methanol and stained with 0.03% methylene blue (Sigma-Aldrich). The number of tumor foci were then counted.

Respiratory hyperoxic therapy

Mice presenting 4T1 tumors were randomly selected to receive either normoxia (21% oxygen) or hyperoxia (60% oxygen) treatment on day 7, when primary tumors became palpable, until the end of the experiment (day 28), as previously reported [27]. Of note, the mice were randomized according to the tumor size to ensure similar tumor sizes at baseline when treatment started. The two treatment groups were then placed in a custom-built chamber (Biospherix; Redfield, NY, USA), which was connected to a supply of oxygen (O_2) gas. The compact oxygen controller, ProOx P110 (Biospherix), was used to ensure that the desired levels of oxygen were maintained inside each chamber throughout the experimental procedures.

Flow cytometry analysis

On day 0, 7, 14, 21, and 28, cleanly excised primary tumors and lungs were placed in petri dishes, and were minced finely with a scalpel blade, then digested, filtered, and washed as described in the *Clonogenic Assay for the Evaluation of Spontaneous Lung Metastasis* section to obtain unicellular suspensions of tissues. The entire spleen was passed through a 70 µm cell strainer and pressed with a plunger. Total BM cells were freshly isolated from the femurs and tibias by flushing with 1 × PBS. After single-cell suspensions of spleen, blood (anticoagulant), and BM were prepared, red blood cells were removed with red blood cell (RBC) Lysis Buffer (ThermoFisher Scientific; Waltham, MA, USA) according to the manufacturer's protocol.

The cell suspensions mentioned above were incubated with anti-mouse BD Fc Block (anti-CD16/32 clone 2.4G2; BD Biosciences) for 10 minutes at 4°C. Afterward, the cells were stained with the following fluorophore-conjugated antibodies for 40 minutes at 4°C: CD45-PE-Cy7, CD3-PE, CD4-APC-Cy7, CD8-PerCP-Cy5.5 (PC5.5), Gr-1-PerCP, CD11b-APC-Cy7, and PD-L1-PE and/or the respective PE-conjugated, isotype-matched control IgGs (ThermoFisher Scientific). The labeled cells were washed twice with staining buffer (BD Biosciences) and were analyzed on a CytoFLEX Flow Cytometer

(Beckman Coulter; Brea, CA, USA) using the FlowJo software (FlowJo LLC; Ashland, OR, USA). MDSCs were gated as $CD45^+Gr\text{-}1^+CD11b^+$ cells, and the percentage of MDSCs in $CD45^+$ cells and in the total population of tissue cells (or total leukocytes from blood, BM, and spleen) was calculated, as dissecting out the organs changed their cell content and number. T-cells were gated as $CD45^+CD3^+$ cells and PD-$L1^+$ cells were gated using isotype control antibodies as described in Figure S4.

Evaluation of hypoxic tissue

A Hypoxyprobe™-1 Plus Kit (Hypoxyprobe, Inc.; Burlington, MA, USA) was used to detect hypoxia in tissues [28]. The hypoxyprobe-1, also named as pimonidazole HCl, is activated in hypoxic cells and forms stable covalent adducts with the thiol groups of proteins, peptides, and amino acids [28]. The anti-hypoxyprobe fluorescein isothiocyanate (FITC)-labeled antibody against pimonidazole (MAb1), which is also included in the kit, binds to these adducts, allowing their detection using immunohistochemical (IHC) procedures (Figure S2). On day 7, BALB/c mice with established 4T1 tumors were treated with 60% oxygen (hyperoxia) or maintained at 21% oxygen (normoxia) treatment for 7 days (day 14) and 21 days (day 28). Treated mice were then injected intraperitoneally (IP) with 80 mg/kg of Hypoxyprobe-1 and primary tumors and lungs were harvested 1.5 hours later to be processed for IF staining with MAb1.

Immunofluorescence (IF) staining

Primary tumors and tumor-bearing lungs from 28-day 4T1 TNBC mice, as well as 0-day mice lungs were harvested after being injected with Hypoxyprobe-1 as described above. Tissues were then embedded in optimal cutting temperature (OCT) compound and frozen in liquid nitrogen. Tissue sections were cut at a thickness of 5 μm, fixed in acetone solution, and pretreated with Peroxidase Block (Dako/Agilent technologies, Inc.; Santa Clara, CA, USA). After washing with 1 × PBS, the sections were incubated with 3% BSA at room temperature for 30 minutes, followed by incubation of antibodies against Gr-1 (ThermoFisher Scientific), PD-L1 (ThermoFisher Scientific), and FITC-conjugated MAb1 against Hypoxyprobe-1 at a dilution of 1:100 at 4°C overnight. Additionally, Alexa Fluor®594-conjugated fluorescent secondary antibody (Abcam; Cambridge, UK) was added to the slides the next day. Finally, the slides were washed and counterstained with 4',6-diamidino-2-phenylindole (DAPI, Sigma-Aldrich). Tissue sections were imaged under a Zeiss fluorescence microscope (Carl Zeiss; Jena, Germany) and were analyzed using four or five random fields per sample.

Statistical analysis

Statistical significant differences in survival were calculated using the log-rank (Mantel-Cox) test, and the differences in tumor size were evaluated suing two-way ANOVA analysis. Statistical significant differences in clones, IHC, and flow cytometry analysis were evaluated using the Student's T-test. Statistical significances were defined as a P value less than (<) 0.05.

Results

4T1-derived tumor progression follows a consistent time course with distinct premetastatic and metastatic phases

Given that BALB/c female mice bearing 4T1 cells developed highly aggressive TNBC with lung metastases (**Figure 1A**), we first investigated the time course it took for the spontaneous metastasis to occur. Clonogenic assays readily detected metastatic tumor cells in the lungs of mice bearing 4T1 tumors at day 21, while there was no evidence of tumor metastases to the lungs at day 7 or even at day 14 (**Figure 1B**). Notably, at day 28, clonogenic assays were not suitable for tumor detection, given the high number of tumor cells present. These findings were confirmed upon gross examination of lung lesions by staining lung tissue sections with H&E (**Figure 1C**). A number of malignant cell clusters were detected in the H&E-stained lung sections of tumor-bearing mice at day 28. Malignant cell groups (arrows in **Figure 1**) were also observed in the lung tissue at day 21, whereas, in accordance to the clonogenic assay results, no tumor cells were found in the lungs of tumor-bearing mice at day 7 and day 14 (**Figure 1B** and **1C**). A previous study reported that tumor cells migrated to the lungs 16 to 18 days after 4T1 cell inoculation [29]. Based on this evidence and our results, we divided the time course it took to develop lung metastases in the 4T1 TNBC model into two

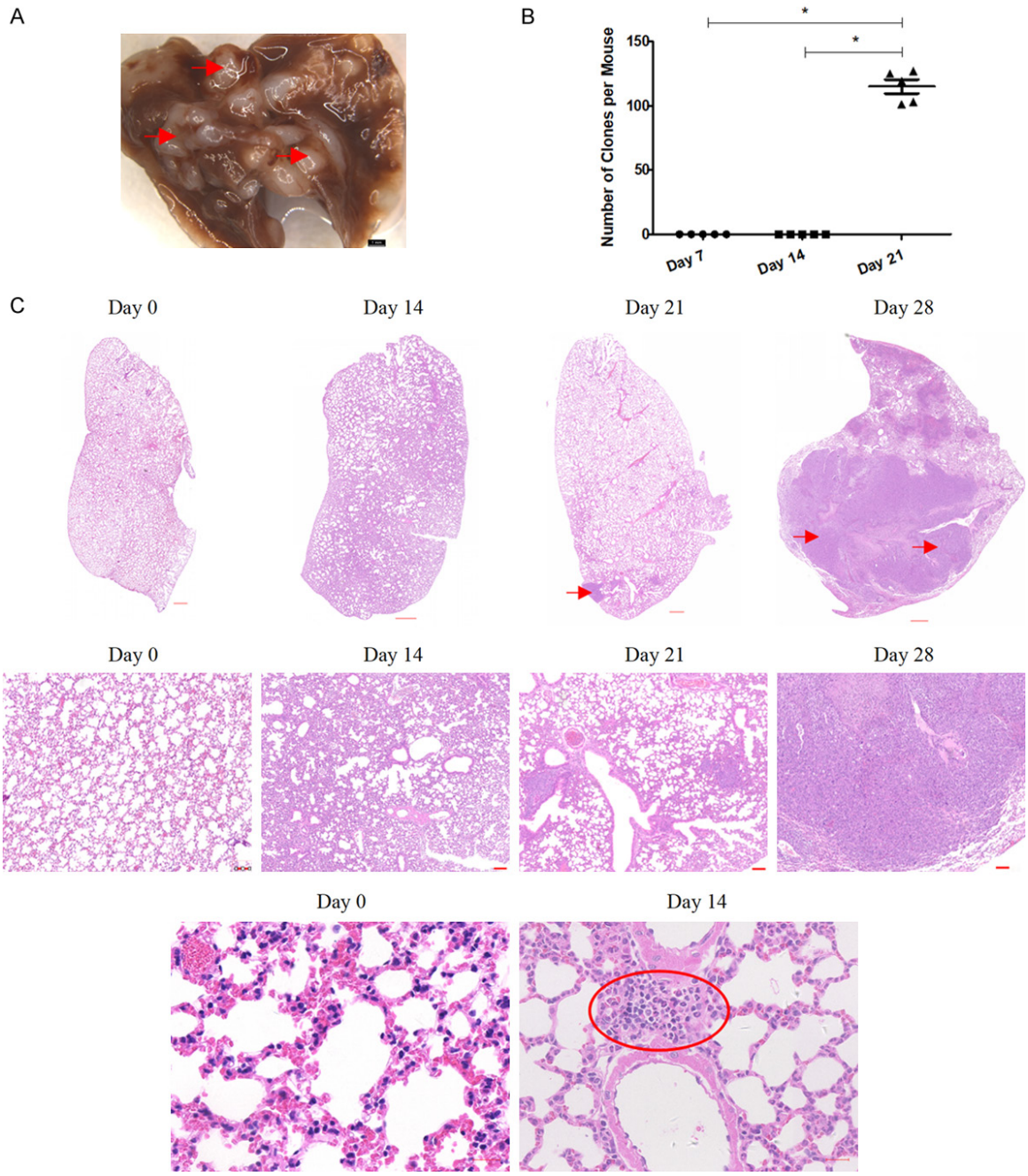

Figure 1. Time course for lung metastases in the 4T1 mammary carcinoma mouse model of triple negative breast cancer (TNBC). A. Representative photograph of the 4T1 mouse lungs with a high tumor burden after TNBC metastasis. Representative tumors are marked by arrows; scale bar = 1 mm. B. Clonogenic analyses of 4T1 cell colonies per lung. Mean values ± standard error of the mean (SEM), n = 5 mice per treatment group. *$P < 0.05$. C. Representative images of hematoxylin and eosin (H&E)-stained lung sections. Tumor metastases are indicated by arrows. The region of inflammatory aggregation is indicated by the red oval. Upper panels, scale bar = 500 μm; middle panels, scale bar = 100 μm; low panels, scale bar = 20 μm. These data are representative of at least three independent experiments.

phases: the premetastatic phase (day 0 to day 14) and the metastatic phase (day 15 to day 28), respectively.

Moreover, the results of our histopathological examination revealed obvious inflammatory cell infiltration around the pulmonary alveoli at

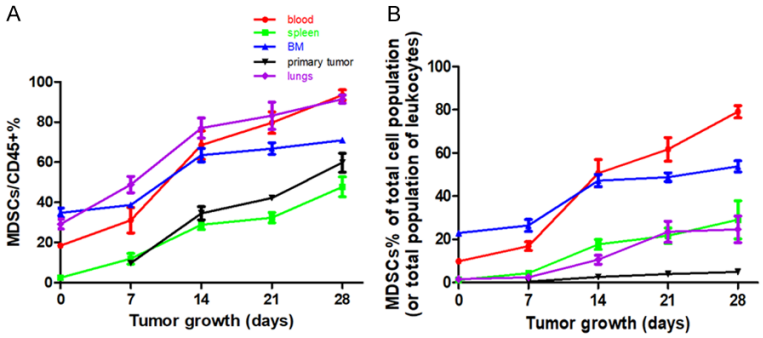

Figure 2. Time-dependent and tissue-specific expansion of myeloid-derived suppressor cells (MDSCs) in 4T1 mice. Flow cytometry analysis of Gr-1$^+$CD11b$^+$ MDSCs in the blood, spleen, bone marrow (BM), lungs, and primary tumor harvested on day 7, day 14, day 21, and day 28 from 4T1 tumor-bearing mice, compared with day 0 non-tumor bearing mice. Percentage of MDSCs in the CD45$^+$ cell population (A) and in the total cell population (or the total leukocyte population) (B). Mean values ± standard deviation (SD). Each experiment was repeated three times (n = 3).

day 14, when compared with tumor-free mice at day 0 (see lymphocyte aggregation in **Figure 1C**), indicating an altered TME in the distant metastatic organ, despite the fact that there was no dissemination of tumor cells from the primary lesion. Based on the absence of metastatic tumor cells and the highly inflammatory conditions observed, the lungs of 4T1 tumor-bearing mice at day 14 were called premetastatic lungs, while those at day 21 and day 28 were considered metastatic lungs.

MDSCs are important TME components in 4T1 mice

MDSCs are known to be major components of the immunosuppressive TME [9]. To determine when and to what extent MDSCs expansion occurs during tumor progression in the 4T1 mouse model, we used flow cytometry analysis to evaluate the frequency of MDSCs (known as Gr-1$^+$CD11b$^+$ cells in mice) in the primary tumor, as well as in the different organs affected by tumor metastasized growth (**Figure 2A** and **2B**). Given that dissecting out the organs can change their cell content and number, we calculated the percentage of MDSCs in the CD45$^+$ cell population (**Figure 2A**) as well as in the total cell population of the affected tissues (i.e., primary tumor in the breast and in the lungs) or in the total leukocyte cell population of blood samples, and other hematopoietic organs (i.e., the BM and the spleen; **Figure 2B**). Consistent trends have been observed using this approach and using both calculation methods. Notably, the expansion of MDSCs occurred in an organ-specific manner as the tumor progressed. When comparing day 28 4T1 tumor mice with day 0 mice, the largest number of MDSCs gains were found in the spleen and the lung. Markedly, there was a 24.6-fold and 15-fold increase in the percentage of MDSCs in the total population of leukocytes in the spleen or in the total population of lung cells, respectively. The increase in the percentage of MDSCs in the total population of blood leukocytes and BM leukocytes was more moderate, as we only observed an 8-fold and 2.3-fold increase in the number of MDSCs found in the blood and BM, respectively. In addition, the percentage of primary tumor-infiltrating MDSCs out of the total number of cells gradually increased over time, from 0.47% at day 7 to 4.9% at day 28 (**Figure 2B**).

Furthermore, MDSCs were found in more than half of the CD45$^+$ cells in all organs (blood, spleen, BM, and lung) and primary tumors of 4T1 mice at day 28 (**Figure 2A**), accounting for as many as 80% of blood leukocytes, 70% of BM leukocytes, 40% of spleen leukocytes, up to 30% of the total population of lung cells, and only 5% of the total primary tumor cells (**Figure 2B**). Notably, we observed the presence of MDSCs in the lungs after 4T1 cell injection as early as day 7, long before tumor cell metastasis (day 15 to day 28; **Figure 1**).

Overall, the expansion of MDSCs in the 4T1 mouse model is time-dependent and tissue-specific event. MDSCs appeared in the lungs during the premetastatic phase (day 0 to day 14) long before tumor cells metastasized there, suggesting that primary tumor cells can regulate the expansion and migration of MDSCs from afar.

Recruitment of MDSCs and upregulation of PD-L1 in the hypoxic TME of 4T1 tumor-bearing mice

We next asked whether hypoxia drove the recruitment of MDSCs to the primary tumor and

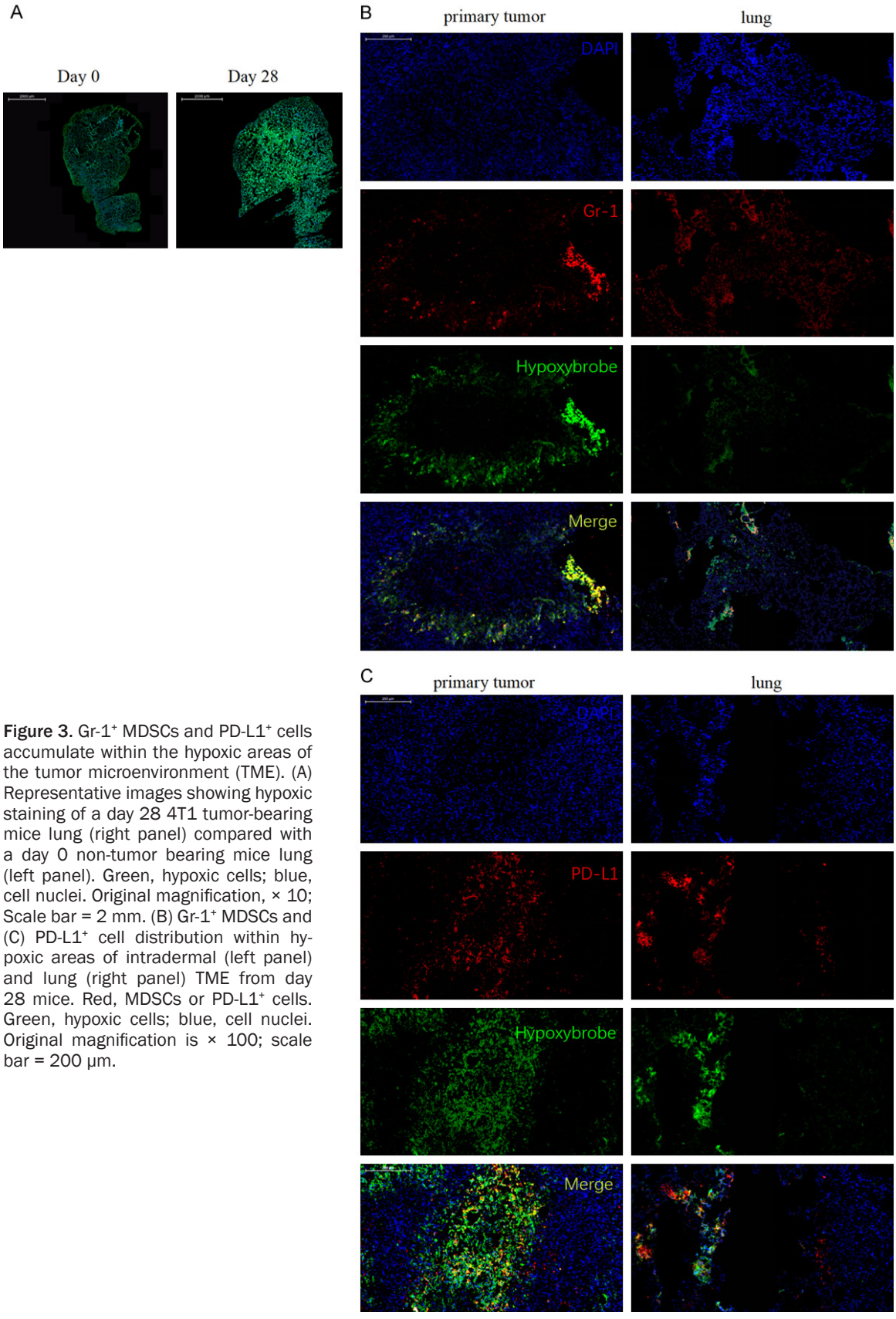

Figure 3. Gr-1$^+$ MDSCs and PD-L1$^+$ cells accumulate within the hypoxic areas of the tumor microenvironment (TME). (A) Representative images showing hypoxic staining of a day 28 4T1 tumor-bearing mice lung (right panel) compared with a day 0 non-tumor bearing mice lung (left panel). Green, hypoxic cells; blue, cell nuclei. Original magnification, × 10; Scale bar = 2 mm. (B) Gr-1$^+$ MDSCs and (C) PD-L1$^+$ cell distribution within hypoxic areas of intradermal (left panel) and lung (right panel) TME from day 28 mice. Red, MDSCs or PD-L1$^+$ cells. Green, hypoxic cells; blue, cell nuclei. Original magnification is × 100; scale bar = 200 μm.

lung metastatic sites in the 4T1 TNBC mouse model. To test this, we stained frozen sections with the myeloid cell marker Gr-1, which detects MDSCs, and the *in vivo* hypoxia marker, Hypoxyprobe, belonging to primary tumors at day 14 and metastatic lungs at day 28. As expected, tumor growth increased the levels of pathophysiological hypoxia in the lung TME of 4T1 tumor-bearing mice, as significantly stronger Hypoxyprobe fluorescence staining was observed in lungs harvested from day 28 4T1 tumor-bearing mice, when compared with lungs harvested from day 0 mice (**Figure 3A**). Analysis of the different anatomical locations of the primary tumor and lung sections showed that Gr-1$^+$ MDSCs preferentially infiltrated more hypoxic areas of tumor and lung metastases (**Figure 3B**).

We next looked at the expression levels of the PD-L1 protein, another important factor regulated by hypoxia in these regions [8]. For this, we first used IF to detect the PD-L1$^+$ cell distribution within the primary tumor and lung TME. In our analysis, we found that PD-L1 and Hypoxyprobe staining patterns significantly overlapped, with an increased number of PD-L1$^+$ cells present in hypoxic tissues relative to normoxic tissues (**Figure 3C**). These data suggest that PD-L1 expression is tightly related to hypoxia in our TNBC mouse model.

Moreover, it has been reported that PD-L1 is upregulated in several of the cell types residing in the TME, including MDSCs [8]. We then investigated the changes in PD-L1 expression levels in MDSCs infiltrates in the TME (**Figure 4**). Day 14, 21, and 28 primary tumors and lungs were harvested from 4T1 cell injected mice, and then analyzed for cell expression of PD-L1 on MDSCs. As shown in **Figure 4A** and **4B**, the percentage of PD-L1$^+$ cells among primary tumor-infiltrating MDSCs at day 28 (41.6%) was significantly higher than at day 14 (24.4%), and day 21 (30.9%). Moreover, upregulation of PD-L1 expression in MDSCs was observed in both premetastatic lungs (day 14) and metastatic lungs (day 28), when compared with lungs from day 0 mice (**Figure 4A** and **4B**). The percentages of PD-L1$^+$ cells in lung-infiltrating MDSCs from 4T1 tumor-bearing mice at days 14 (22.7%), 21 (29.8%), and 28 (42%) were all significantly higher than those from day 0 mice (4.6%). Overall, the expression levels of PD-L1 in tumor-infiltrating MDSCs and lung-infiltrating MDSCs were both increased over time and significantly augmented in the later phases of tumor growth and metastasis.

In order to determine whether PD-L1 expression on 4T1 tumor cells was upregulated *in vitro*, we analyzed the 4T1 mammary carcinoma cell cultures used to inoculate the TNBC mouse model in this study. In addition, 4T1 tumor cells derived from primary tumors *in vivo* were tested for PD-L1 expression using flow cytometry techniques. To this end, we gated 4T1 tumor cells from *in vivo* primary tumor single-cell suspensions as large CD45 negative cells and evaluated the PD-L1 expression levels induced within the TME, as with MDSCs above. Particularly, high expression levels of PD-L1 were observed in the 4T1 tumor cells collected *in vivo*, when compared to the 4T1 cell cultures *in vitro*. Markedly, the percentage of PD-L1$^+$ cells obtained from the 4T1 cells collected *in vivo* consistently increased over time (**Figure 4C** and **4D**).

Collectively, our results demonstrate that lung oxygen levels decrease after lung metastasis in the 4T1 tumor bearing mice. Additionally, hypoxic conditions appear to be major drivers of MDSC recruitment and PD-L1 upregulation in the TME.

Antitumor T-cell immunity suppression in the TME of 4T1 tumor-bearing mice

We next studied the roles increased MDSC frequency and PD-L1 expression, may have on regulating antitumor immunity in the hypoxic TME. On days 0, 14, 21, and 28 after 4T1 cell injections, primary tumors and lungs were harvested from injected mice and analyzed in order to identify the frequency of tumor-infiltrating and lung-infiltrating CD4$^+$ T-cells, CD8$^+$ T-cells, and T-cells. Furthermore, flow cytometry time course assay analysis showed that hypoxia inhibited the accumulation of T-cells in both the lung and primary TME (**Figure 5**). In the metastatic phase (i.e., day 21 and day 28), the percentage of CD4$^+$ and CD8$^+$ T-cells among the total population of T-cells, as well as the percentage of CD4$^+$, CD8$^+$ T-cells, and the total population of T-cells among the total population of pulmonary cells, showed a marked decrease, when compared with day 0 mice, especially on day 28 of the metastatic phase (**Figure 5A** and **5B**). In contrast, we did not observe

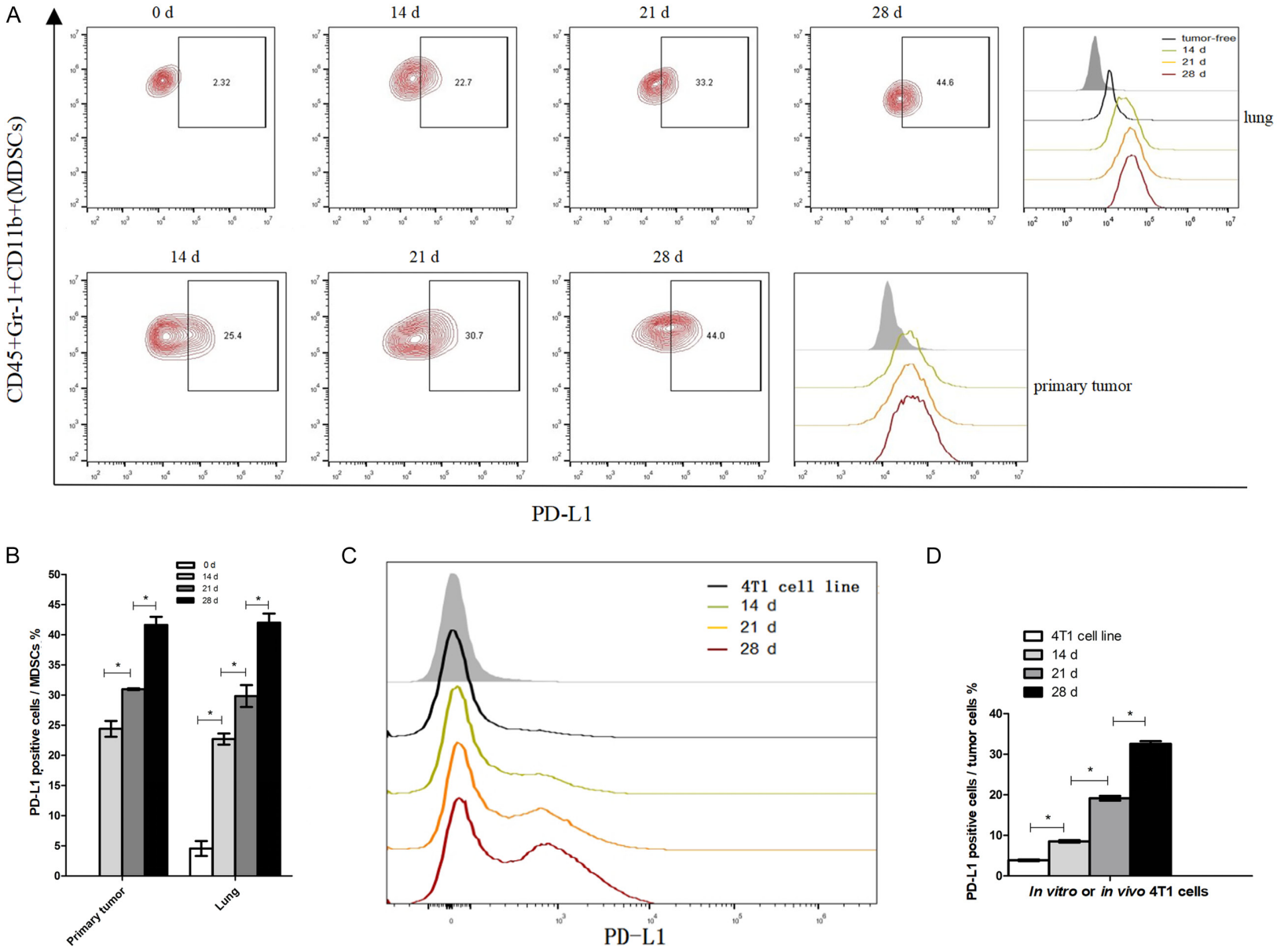
A
0 d
14 d
21 d
28 d
2.32
22.7
33.2
44.6
tumor-free
14 d
21 d
28 d
lung
14 d
21 d
28 d
25.4
30.7
44.0
primary tumor
CD45+Gr-1+CD11b+(MDSCs)
PD-L1
B
0 d
14 d
21 d
28 d
PD-L1 positive cells / MDSCs %
Primary tumor
Lung
C
4T1 cell line
14 d
21 d
28 d
PD-L1
D
4T1 cell line
14 d
21 d
28 d
PD-L1 positive cells / tumor cells %
In vitro or in vivo 4T1 cells

Figure 4. Upregulation of PD-L1 in MDSCs and tumor cells of 4T1 tumor-bearing mice. A. Left: Percentage of PD-L1$^+$ cells among MDSCs obtained from lung metastases and primary tumors at the indicated times. Right: Representative histograms depicting the surface expression of PD-L1 in MDSCs compared with the isotype control (shaded histogram). B. Statistically significant differences (indicated by asterisks) in the proportion of PD-L1$^+$ cells among MDSCs (n = 3 mice per group). C. Representative histograms depicting the surface expression levels of PD-L1 in cultured 4T1 cell line (*in vitro*) and in *in vivo* derived 4T1 tumor cells compared with the isotype control (shaded area). D. Statistically significant differences in the percentage of PD-L1$^+$ cells between cultured and *in vivo* derived 4T1 tumor cells (n = 4 mice per group). *$P < 0.05$; Mean values ± SEM. Each experiment was repeated three times (n = 3).

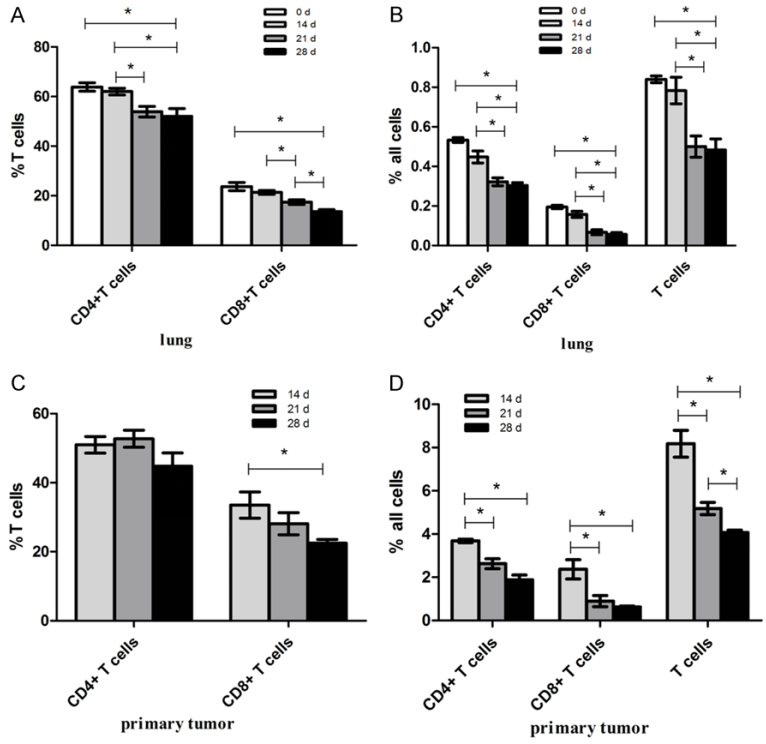

Figure 5. Reduction of T-cells in the primary tumor and lung TME. T-cells were gated as CD45$^+$CD3$^+$ cells. Results show the percentages of CD4$^+$ T-cells and CD8$^+$ T-cells in respect to (A) lung-infiltrating and (C) tumor-infiltrating total population of T-cells, as well as the percentages of (B) lung-infiltrating and (D) tumor-infiltrating CD4$^+$ T-cells, CD8$^+$ T-cells, and the total population of T-cells relative to the total population of the tissue cells. *$P < 0.05$; n = 5 mice. Mean values ± SEM. Each result was repeated three times (n = 3).

a significant difference in the percentages of CD4$^+$, CD8$^+$, or total T-cells in premetastatic lungs (day 14) and tumor-free (0 day) lungs (**Figure 5A** and **5B**). Markedly, the percentage of both primary tumor-infiltrating CD4$^+$ and CD8$^+$ T-cells gradually decreased with the growth of the primary tumor (**Figure 5C** and **5D**). Together these data led us to conclude that as the primary tumor progresses, increased levels in PD-L1 expression and in the frequency of MDSC associated with hypoxia, result in the conversion of the TME into an immunosuppressive environment in primary tumors and metastatic lungs.

Respiratory hyperoxia enhances antitumor T-cell immunity by inhibiting PD-L1 expression and the recruitment of MDSCs

Based on data indicating that hypoxia drives MDSC accumulation and PD-L1 upregulation in the TME, which decreases lung infiltration of T-cells, we hypothesized that respiratory hyperoxia therapy may be able to counteract these effects. To test this, mice were placed in chambers supplied with well-controlled, 60% or 21% oxygen levels (normoxia or hyperoxia, respectively), on day 7 after the inoculation of 4T1 cells, until the completion of the study on day 28. This was based on 4T1 tumors being palpable between day 5 and day 7 (Figure S1A), and on the increased presence of MDSCs, which could be detected in the lungs as early as 7 days after injection (**Figure 2**). **Figure 6A** shows less hypoxic conditions after Hypoxyprobe staining in the lungs of tumor-bearing 4T1 mice treated with hyperoxia therapy at day 28, when compared to the lungs of tumor-bearing 4T1 mice treated with normoxia at day 28. This demonstrated that respiratory hyperoxia can, indeed, decrease lung TME hypoxic conditions.

We next examined whether treating 4T1 mice with hyperoxia could affect the recruitment of MDSCs to different organs. Our results showed that during the premetastatic phase (i.e., day 14), respiratory hyperoxia therapy can lead to a significant decrease in the frequency of MDSCs in the primary tumor, spleen, and lungs of 4T1

A

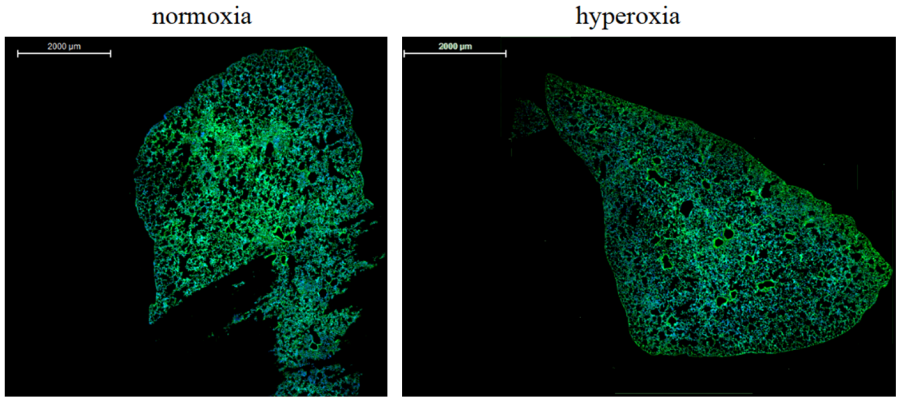
normoxia
hyperoxia
2000 μm
2000 μm

B

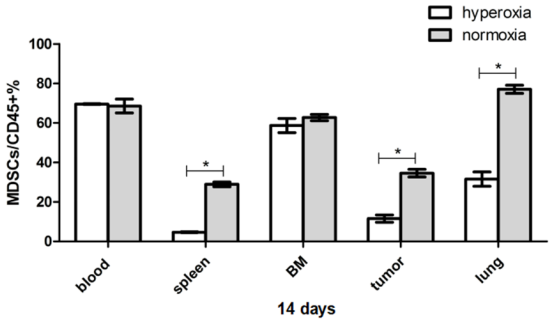
hyperoxia
normoxia
MDSCs/CD45+%
blood
spleen
BM
tumor
lung
14 days

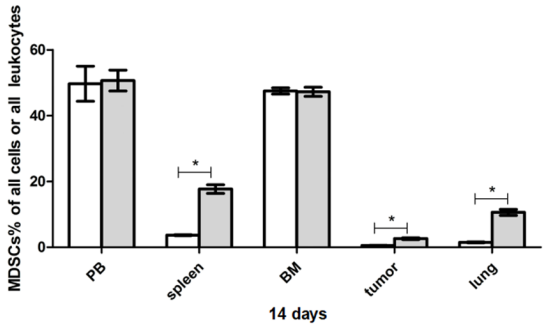
MDSCs% of all cells or all leukocytes
PB
spleen
BM
tumor
lung
14 days

C

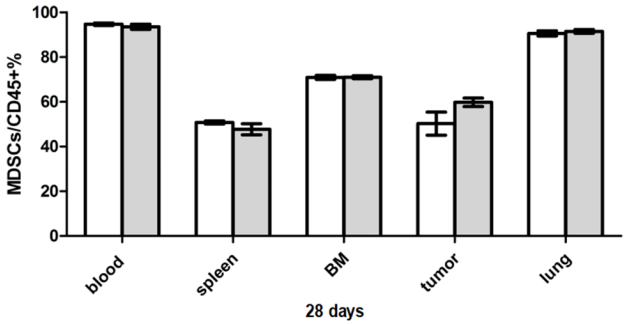
MDSCs/CD45+%
blood
spleen
BM
tumor
lung
28 days

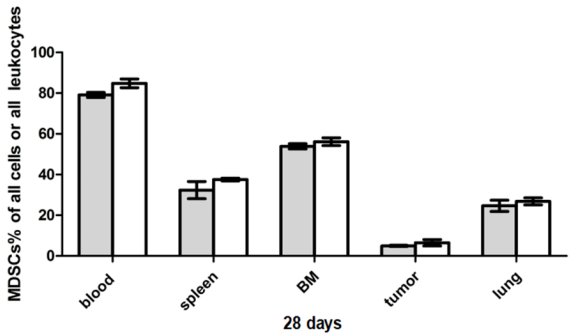
MDSCs% of all cells or all leukocytes
blood
spleen
BM
tumor
lung
28 days

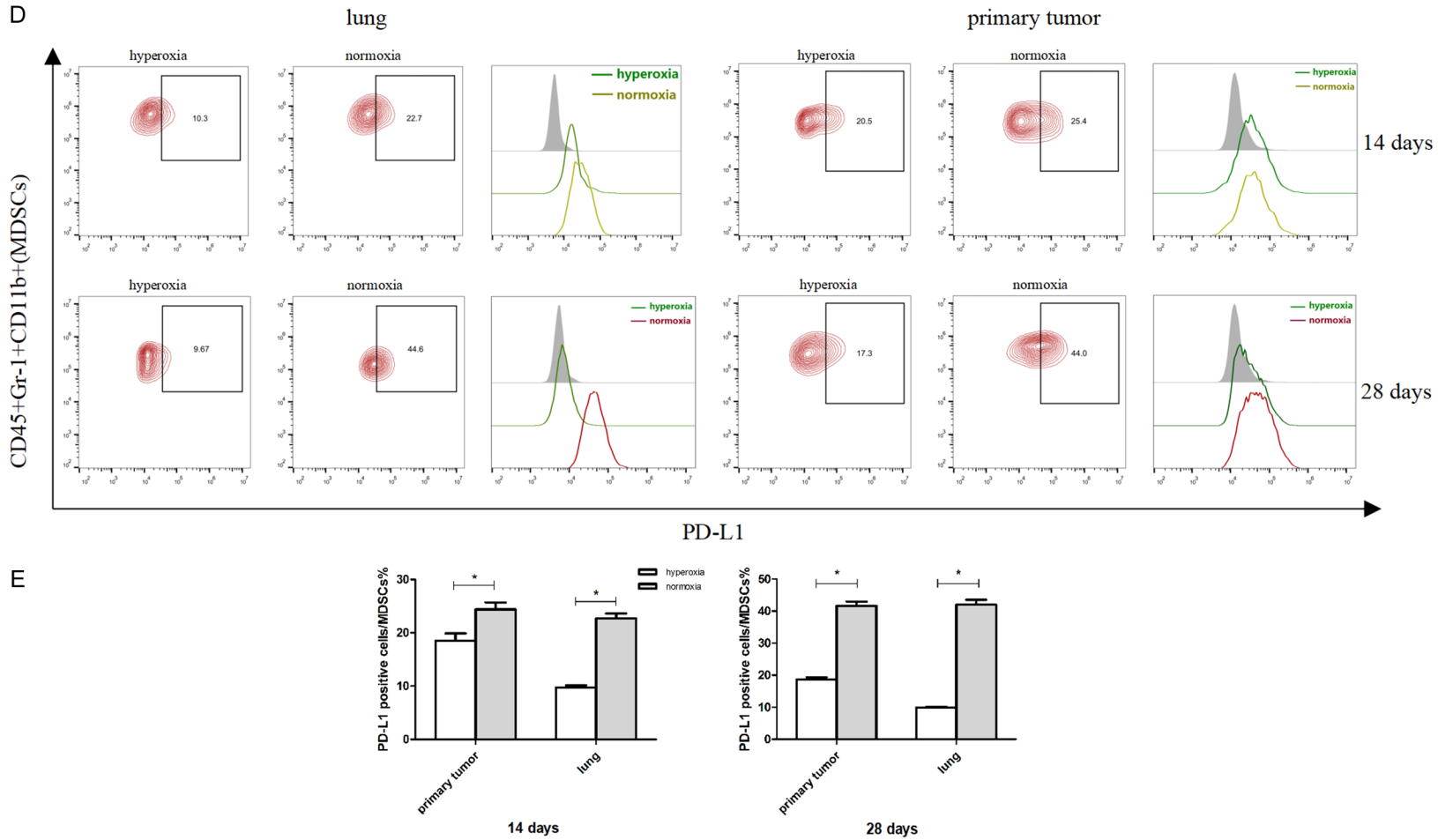

Figure 6. Respiratory hyperoxia inhibits MDSCs recruitment and PD-L1 expression in the 4T1 mouse model of TNBC. (A) Respiratory hyperoxia decreases tumor-associated hypoxia in the lungs. Green, hypoxic areas; blue, cell nuclei. Scale bar = 2 mm. Respiratory hyperoxia differentially changes the frequency of MDSCs in various organs at (B) day 14 and (C) day 28. n = 4 mice per group. (D and E) Respiratory hyperoxia decreases PD-L1 expression in lung-infiltrating and tumor-infiltrating MDSCs. n = 3 mice per group. $*P < 0.05$. Mean values ± SEM. Each result was repeated three times (n = 3).

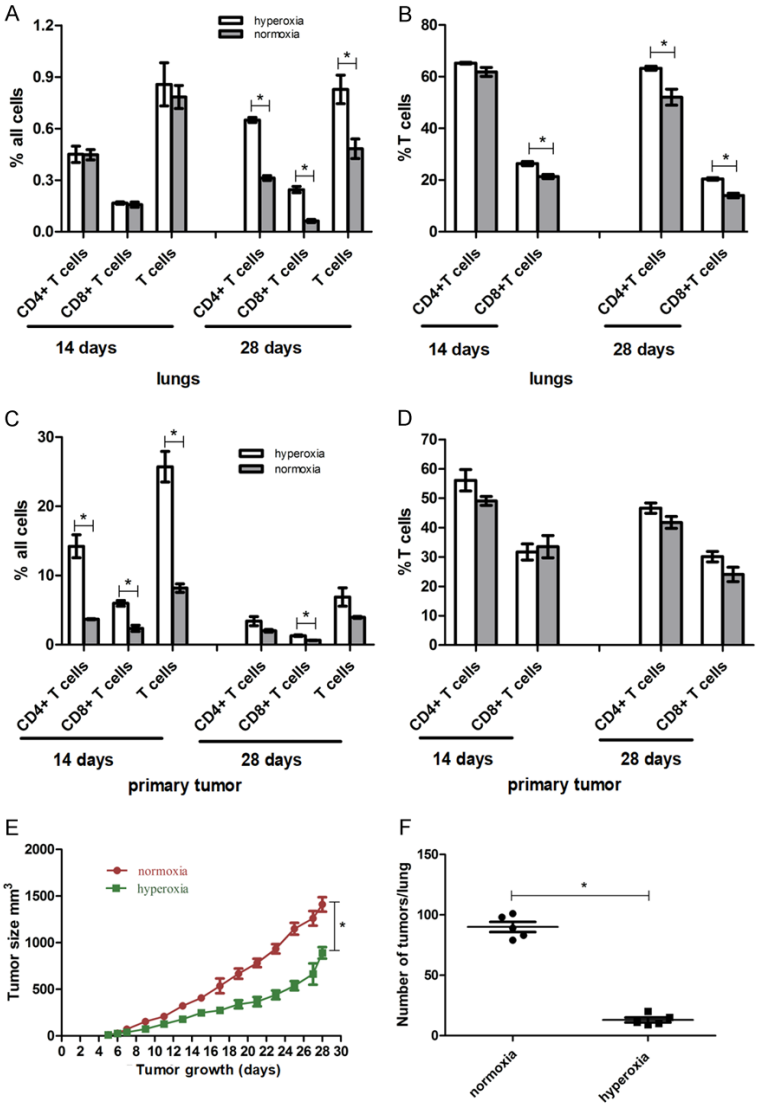

Figure 7. Respiratory hyperoxia increases T-cell accumulation, inhibiting primary tumor growth and the incidence of lung metastasis in the 4T1 mouse model of TNBC. (A) Percentage of lung-infiltrating and (C) tumor-infiltrating $CD4^+$ T-cells, $CD8^+$ T-cells, and total population of T-cells in relation to total tissue cell population from normoxia and hyperoxia treatment groups. (B) Percentages of lung-infiltrating and (D) tumor-infiltrating $CD4^+$ T-cells and $CD8^+$ T-cells among T-cells. *$P < 0.05$; n = 4 mice. Mean values ± SEM. (E) Respiratory hyperoxia inhibits primary tumor growth and (F) lung metastases in mice treated with hyperoxia therapy (60% oxygen levels), when compared with mice treated with normoxia therapy (21% oxygen levels). *$P < 0.05$; n = 5 mice; Mean values ± SEM. Each experiment was repeated three times (n = 3).

tumor bearing mice, when compared with their normoxia treated counterpart. Notably, these observations were not seen in the blood and BM samples of treated animals (**Figure 6B**). In contrast, we found no differences in the frequency of lung- or tumor-infiltrating MDSCs between the mice groups treated with hyperoxia and normoxia conditions during the metastatic phase (i.e., day 28) (**Figure 6C**). Naturally, we were intrigued to see a significant reduction of PD-L1 expression in primary tumor-infiltrating MDSCs in tumor-bearing 4T1 mice, when treated with hyperoxic conditions during both premetastatic and metastatic phases (**Figure 6D** and **6E**).

Additional flow cytometric analysis indicated that respiratory hyperoxia treatments resulted in an increase of T-cell infiltration in tumor and lung tissues (**Figure 7**). An increase in the percentages of $CD8^+$, $CD4^+$, and the total population of T-cells in relation to the total cell population obtained from the hyperoxia treated mouse group was observed in lung-infiltrating T-cells during the metastatic phase (i.e., day 28), when compared with mice from the normoxia treated group. However, during the premetastatic phase (i.e., day 14), no significant changes in the hyperoxia treated group were observed (**Figure 7A**). Interestingly, we also observed a variation in the response to hyperoxia treatments between $CD4^+$ and $CD8^+$ T-cells. The percentage of $CD8^+$ T-cells among the total T-cell population in the lung TME was affected during both the premetastatic and metastatic phases, while the $CD4^+$ T-cell population was only affected during the metastatic phase. In addition, there were more significant changes observed in the $CD8^+$ T-cell population, compared to the $CD4^+$ T-cell population of the lung TME (**Figure 7B**).

The percentages of $CD4^+$ and $CD8^+$ T-cells, as well as the percentage of the total population of T-cells among all cells of the TME found in primary tumor-infiltrating T-cells, increased in the hyperoxia treated group during the premet-

astatic phase (i.e., day 0 to day 14). Only the percentage of $CD8^+$ T-cells among all cells showed a hyperoxia-mediated increase during the metastatic phase (i.e., day 28; **Figure 7C**); while the percentages of $CD4^+$ T-cells and $CD8^+$ T-cells among all T-cells were not affected during either the premetastatic or metastatic phase (**Figure 7D**). Of note, the effects seen on $CD4^+$ and $CD8^+$ T-cells might be a result of different regulatory mechanisms - and possibly not all through hypoxic conditions.

Nevertheless, our data provide evidence that respiratory hyperoxia treatments are able to decrease tissue hypoxia in the TNBC 4T1 mouse model, which in turn prevents the suppression of antitumor T-cell immunity by inhibiting the expansion of MDSCs and upregulation of the PD-1/PD-L1 pathway. However, hyperoxia treatments alone, are unable to induce a long-lasting decrease of infiltrated MDSCs in the TME.

Respiratory hyperoxia therapy has antitumor effects

We next tested whether respiratory hyperoxia could have an inhibitory effect on the growth of lung metastases in the 4T1 TNBC mouse model. To this end, hyperoxia treatments consisting of 60% oxygen were delivered to mice on day 7 after 4T1 cell inoculation, before metastasis to the lungs took place. Our results showed that respiratory hyperoxia treatments could inhibit tumor growth slightly, with none of the mice showing a complete regression of primary tumors (**Figure 7E**). Nevertheless, in lung tissue, we found that hyperoxia treatment could induce a strong regression of lung metastases on day 28 (**Figures 7F** and S3). Importantly, the number of lung metastatic modes fell from 90 per lung in the normoxic treated group to 13 per lung in the hyperoxic treated group ($P < 0.05$). Hyperoxia therapy can then be seen as an effective means of overcoming immunosuppression in the TME, given our data demonstrating tumor growth and lung metastases regulation in the 4T1 mouse model of TNBC.

Discussion

Hypoxia plays a pivotal role in regulating both tumor and immune cell functions, especially related to immunosuppressive processes [4]. It has been shown that respiratory hyperoxia therapy can increase oxygen content in the hypoxic TME and thereby improve the effectiveness of conventional anti-tumor treatments [14]. Nonetheless, the molecular mechanisms underlying the relationship between respiratory hyperoxia and tumor immunity remains unclear. Based on the anti-tumor potential that respiratory hyperoxia has demonstrated in previous studies, we sought to investigate its effectiveness and underlying molecular pathways in inhibiting metastases and in restoring tumor immunity of a metastatic organ in a TNBC model.

In our study, a 4T1 mouse model of TNBC showed a tumor-dependent and organ-specific expansion of MDSCs in multiple organs, demonstrating that MDSCs are key components of the TME. In addition, increased levels of pathophysiological hypoxia in the lung TME accounted for most of the tissue area in the 4T1 mouse model. Interestingly, the frequency of MDSCs and PD-L1 expression levels changed according to the levels of hypoxia, not only in the primary tumor TME, but also in the metastatic lung TME. Thus, the frequency of MDSCs and PD-L1 expression levels may serve as biomarkers for the detection of hypoxia in the TME. Compared with traditional markers such as HIF-1a, which are assessed by IHC [1, 30], the frequency of MDSCs and PD-L1 expression as biomarkers, represent not only the level of hypoxia, but also the levels of hypoxia-induced immunosuppression.

Our results showed important modifications of the premetastatic lung TME, not only the recruitment of MDSCs, but also an increased expression of PD-L1 levels in MDSCs. These findings are consistent with previous reports showing that MDSCs accumulate to form a premetastatic niche in the premetastatic lung and brain, but not in other organs [26, 31]. Here, we speculate that the changes observed in our study are also lung specific and may contribute to the fact that the lungs are a preferential metastatic site of the 4T1 TNBC mouse model. We plan to confirm this in a future study. However, our data also showed that lung-infiltrating T-cells are not as affected in the premetastatic phase as they are in the metastatic phase, suggesting that metastasized tumor cells to the lungs can affect T-cell accumulation in the TME. We speculate that this could be due to changes in the cytokine/chemokine tumor profile and also ch-

anges in the expression of chemokine receptors on T-cells after the arrival of tumor cells to the lungs.

In our study, respiratory hyperoxia treatments weakened the MDSC- and PD-L1-mediated immunosuppression of the primary tumor and lung metastases in the 4T1 TNBC mouse model. However, hyperoxia treatments alone could not decrease lung-infiltrating or tumor-infiltrating MDSCs at the end of our study (i.e., day 28), likely because of the excessive production and recruitment of MDSCs in hematopoietic organs at day 28, thus preventing hyperoxia from inducing a long-lasting decrease in MDSC frequency. Other studies suggest changes in the cytokine levels in the TME and changes in the expression of chemokine receptors on MDSCs [7], which is a plausible and important hypothesis for further investigation.

In addition, we observed that $CD4^+$ and $CD8^+$ T-cells were differently affected in the TME of 4T1 tumor-bearing mice when maintained at 21% oxygen levels, compared with day 0 mice. $CD4^+$ and $CD8^+$ T-cells were also differentially affected by respiratory hyperoxia treatments, with more prevalent changes in $CD8^+$ T-cells than in $CD4^+$ T-cells. Other regulatory mechanisms may be involved in the recruitment of $CD4^+$ and $CD8^+$ T-cells to the TME and possibly not all taking place through hypoxic mechanisms. Further studies examining the differences in the expression of chemokine receptors, known as chemokine profiles, in $CD4^+$ and $CD8^+$ T-cell populations are urgently needed. Nonetheless, the therapeutic effects observed in our study from respiratory hyperoxia treatments were strong, although less obvious in T-cells present in primary tumors than in the T-cells identified in the lungs. The limited recovery of T-cell infiltration in the primary tumor may provide an explanation for the limited tumor growth control achieved via hyperoxia therapy in this study.

Overall, our results indicate that respiratory hyperoxia may provide a readily available adjuvant therapy in the prevention and control of lung metastases in TNBC patients. We propose the clinical testing of respiratory hyperoxia either alone or in combination with other immunotherapy treatments in patients with advanced TNBC. Based on the PD-L1 expression level changes obtained with the hyperoxia treatments in our study, we propose that respiratory hyperoxia treatments would be most effective when combined with existing immunotherapy targeting pathways, such as PD-1/PD-L1, providing non-invasive treatment options for metastatic TNBC, which constitute the highest unmet need population in breast cancer patients.

Acknowledgements

This work was supported by the Natural Science Foundation of Guangdong Province [grant number 2016A030310134]; The Young teacher training program of Sun Yat-sen University [grant number 17ykpy26]; and the Science and Technology Planning Project of Guangdong Province [grant number 2014A030304016] of China.

Disclosure of conflict of interest

None.

Abbreviations

TME, tumor microenvironment; PD-1, programmed cell death-1; PD-L1, programmed death-ligand 1; MDSCs, myeloid-derived suppressor cells; TNBC, triple-negative breast cancer; TAMs, tumor-associated macrophages; Treg cells, regulatory T-cells; HIF-1, hypoxia-inducible factor-1; CTLA-4, cytotoxic T-lymphocyte associated protein 4; BM, bone marrow; ATCC, American Type Culture Collection; HBSS, Hank's Balanced Salt Solution; TD, tumor diameters; PBS, Phosphate Buffered Saline; FITC, fluorescein isothiocyanate; MAb1, anti-Hypoxyprobe fluorescein isothiocyanate (FITC)-labeled antibody against pimonidazole (MAb1); DAPI, 4',6-Diamidino-2-Phenylindole, Dihydrochloride.

Address correspondence to: Shenming Wang and Ying Lin, Department of Thyroid and Breast Surgery, The First Affiliated Hospital of Sun Yat-sen University, NO. 58 Zhongshan Road 2, Guangzhou 510080, China. Tel: +86 15876544695; E-mail: wshenm@mail.sysu.edu.cn (SMW); Tel: +86 130-76873871; E-mail: linying3@mail.sysu.edu.cn (YL)

References

[1] Pan Y, Shao D, Zhao Y, Zhang F, Zheng X, Tan Y, He K, Li J, Chen L. Berberine reverses hypoxia-induced chemoresistance in breast cancer through the inhibition of AMPK-HIF-1alpha. Int J Biol Sci 2017; 13: 794-803.

[2] Rankin EB, Giaccia AJ. Hypoxic control of metastasis. Science 2016; 352: 175-180.

[3] Semenza GL. Oxygen sensing, homeostasis, and disease. N Engl J Med 2011; 365: 537-547.
[4] Corzo CA, Condamine T, Lu L, Cotter MJ, Youn JI, Cheng P, Cho HI, Celis E, Quiceno DG, Padhya T, McCaffrey TV, McCaffrey JC, Gabrilovich DI. HIF-1alpha regulates function and differentiation of myeloid-derived suppressor cells in the tumor microenvironment. J Exp Med 2010; 207: 2439-2453.
[5] Flecken T, Schmidt N, Hild S, Gostick E, Drognitz O, Zeiser R, Schemmer P, Bruns H, Eiermann T, Price DA, Blum HE, Neumann-Haefelin C, Thimme R. Immunodominance and functional alterations of tumor-associated antigen-specific CD8+ T-cell responses in hepatocellular carcinoma. Hepatology 2014; 59: 1415-1426.
[6] Motz GT, Coukos G. The parallel lives of angiogenesis and immunosuppression: cancer and other tales. Nat Rev Immunol 2011; 11: 702-711.
[7] Chiu DK, Xu IM, Lai RK, Tse AP, Wei LL, Koh HY, Li LL, Lee D, Lo RC, Wong CM, Ng IO, Wong CC. Hypoxia induces myeloid-derived suppressor cell recruitment to hepatocellular carcinoma through chemokine (C-C motif) ligand 26. Hepatology 2016; 64: 797-813.
[8] Noman MZ, Desantis G, Janji B, Hasmim M, Karray S, Dessen P, Bronte V, Chouaib S. PD-L1 is a novel direct target of HIF-1alpha, and its blockade under hypoxia enhanced MDSC-mediated T cell activation. J Exp Med 2014; 211: 781-790.
[9] Gabrilovich DI, Nagaraj S. Myeloid-derived suppressor cells as regulators of the immune system. Nat Rev Immunol 2009; 9: 162-174.
[10] AiErken N, Shi HJ, Zhou Y, Shao N, Zhang J, Shi Y, Yuan ZY, Lin Y. High PD-L1 expression is closely associated with tumor-infiltrating lymphocytes and leads to good clinical outcomes in chinese triple negative breast cancer patients. Int J Biol Sci 2017; 13: 1172-1179.
[11] Highfill SL, Cui Y, Giles AJ, Smith JP, Zhang H, Morse E, Kaplan RN, Mackall CL. Immunological mechanisms of the antitumor effects of supplemental oxygenation. Sci Transl Med 2015; 7: 230r-277r.
[12] Hatfield SM, Kjaergaard J, Lukashev D, Belikoff B, Schreiber TH, Sethumadhavan S, Abbott R, Philbrook P, Thayer M, Shujia D, Rodig S, Kutok JL, Ren J, Ohta A, Podack ER, Karger B, Jackson EK, Sitkovsky M. Systemic oxygenation weakens the hypoxia and hypoxia inducible factor 1alpha-dependent and extracellular adenosine-mediated tumor protection. J Mol Med (Berl) 2014; 92: 1283-1292.
[13] Daruwalla J, Christophi C. Hyperbaric oxygen therapy for malignancy: a review. World J Surg 2006; 30: 2112-2131
[14] Stuhr LE, Iversen VV, Straume O, Maehle BO, Reed RK. Hyperbaric oxygen alone or combined with 5-FU attenuates growth of DMBA-induced rat mammary tumors. Cancer Lett 2004; 210: 35-40.
[15] Kawasoe Y, Yokouchi M, Ueno Y, Iwaya H, Yoshida H, Komiya S. Hyperbaric oxygen as a chemotherapy adjuvant in the treatment of osteosarcoma. Oncol Rep 2009; 22: 1045-1050.
[16] Ogawa K, Ishiuchi S, Inoue O, Yoshii Y, Saito A, Watanabe T, Iraha S, Toita T, Kakinohana Y, Ariga T, Kasuya G, Murayama S. Phase II trial of radiotherapy after hyperbaric oxygenation with multiagent chemotherapy (procarbazine, nimustine, and vincristine) for high-grade gliomas: long-term results. Int J Radiat Oncol Biol Phys 2012; 82: 732-738.
[17] Ogawa K, Yoshii Y, Inoue O, Toita T, Saito A, Kakinohana Y, Adachi G, Ishikawa Y, Kin S, Murayama S. Prospective trial of radiotherapy after hyperbaric oxygenation with chemotherapy for high-grade gliomas. Radiother Oncol 2003; 67: 63-67.
[18] Jezequel P, Loussouarn D, Guerin-Charbonnel C, Campion L, Vanier A, Gouraud W, Lasla H, Guette C, Valo I, Verriele V, Campone M. Gene-expression molecular subtyping of triple-negative breast cancer tumours: importance of immune response. Breast Cancer Res 2015; 17: 43.
[19] Ye Y, Liu S, Wu C, Sun Z. TGFβ modulates inflammatory cytokines and growth factors to create premetastatic microenvironment and stimulate lung metastasis. J Mol Hist 2015; 46: 365-375.
[20] Dawood S, Rugo HS. Targeting the host immune system: PD-1 and PD-L1 antibodies and breast cancer. Curr Opin Support Palliat Care 2016; 10: 336-342.
[21] Kim K, Skora AD, Li Z, Liu Q, Tam AJ, Blosser RL, Diaz LJ, Papadopoulos N, Kinzler KW, Vogelstein B, Zhou S. Eradication of metastatic mouse cancers resistant to immune checkpoint blockade by suppression of myeloid-derived cells. Proc Natl Acad Sci U S A 2014; 111: 11774-11779.
[22] Gibson J. Anti-PD-L1 for metastatic triple-negative breast cancer. Lancet Oncol 2015; 16: e264.
[23] Schmid P, Adams S, Rugo HS, Schneeweiss A, Barrios CH, Iwata H, Dieras V, Hegg R, Im SA, Shaw WG, Henschel V, Molinero L, Chui SY, Funke R, Husain A, Winer EP, Loi S, Emens LA. Atezolizumab and nab-paclitaxel in advanced triple-negative breast cancer. N Engl J Med 2018; 379: 2108-2121.
[24] Wang HF, Ning F, Liu ZC, Wu L, Li ZQ, Qi YF, Zhang G, Wang HS, Cai SH, Du J. Histone deacetylase inhibitors deplete myeloid-derived suppressor cells induced by 4T1 mammary tu-

mors in vivo and in vitro. Cancer Immunol Immunother 2017; 66: 355-366.
[25] Thiel M, Chouker A, Ohta A, Jackson E, Caldwell C, Smith P, Lukashev D, Bittmann I, Sitkovsky MV. Oxygenation inhibits the physiological tissue-protecting mechanism and thereby exacerbates acute inflammatory lung injury. PLoS Biol 2005; 3: e174.
[26] Liu Y, Komohara Y, Domenick N, Ohno M, Ikeura M, Hamilton RL, Horbinski C, Wang X, Ferrone S, Okada H. Expression of antigen processing and presenting molecules in brain metastasis of breast cancer. Cancer Immunol Immunother 2012; 61: 789-801.
[27] Shang J, Yang YY, Guo XL, Liu HG. Ang II type 1 receptor expression in rat aorta exposed to chronic intermittent hypoxia: effects of p38MAPK and ERK1/2 signaling. Chin Med J (Engl) 2013; 126: 3264-3269.
[28] Raleigh JA, Dewhirst MW, Thrall DE. Measuring tumor hypoxia. Semin Radiat Oncol 1996; 6: 37-45.
[29] Kaplan RN, Riba RD, Zacharoulis S, Bramley AH, Vincent L, Costa C, MacDonald DD, Jin DK, Shido K, Kerns SA, Zhu Z, Hicklin D, Wu Y, Port JL, Altorki N, Port ER, Ruggero D, Shmelkov SV, Jensen KK, Rafii S, Lyden D. VEGFR1-positive haematopoietic bone marrow progenitors initiate the pre-metastatic niche. Nature 2005; 438: 820-827.
[30] Swartz JE, Pothen AJ, Stegeman I, Willems SM, Grolman W. Clinical implications of hypoxia biomarker expression in head and neck squamous cell carcinoma: a systematic review. Cancer Med 2015; 4: 1101-1116.
[31] Yan HH, Pickup M, Pang Y, Gorska AE, Li Z, Chytil A, Geng Y, Gray JW, Moses HL, Yang L. Gr-1+CD11b+ myeloid cells tip the balance of immune protection to tumor promotion in the premetastatic lung. Cancer Res 2010; 70: 6139-6149.

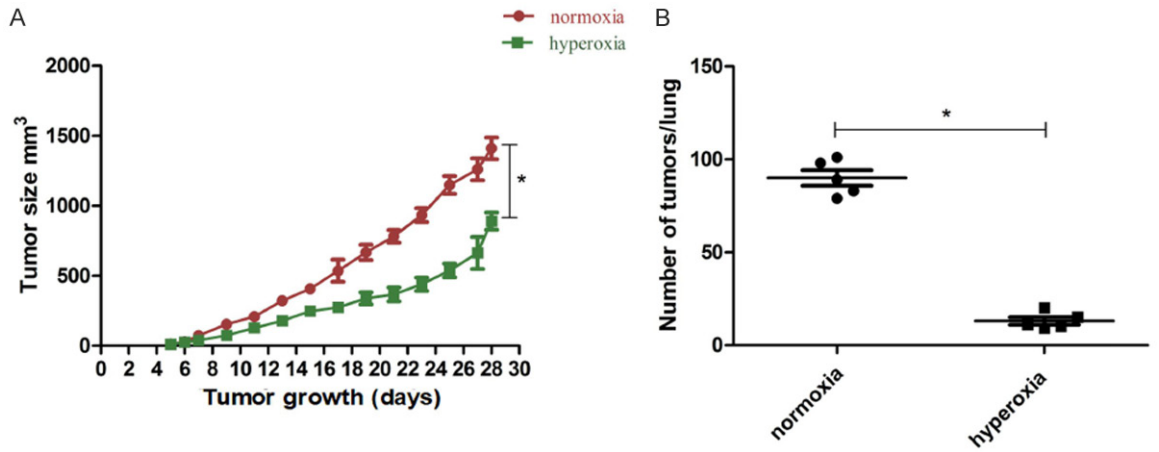

Figure S1. 4T1 cells injected into wild-type BALB/c female mice develop into highly aggressive TNBC with metastases to the lung. A. The primary tumor volumes were calculated as described in the "Materials and Methods" section. n = 5 mice. B. The mice were sacrificed when the tumor diameter reached an average of 14 to 16 mm or when the mice became moribund; n = 6 mice.

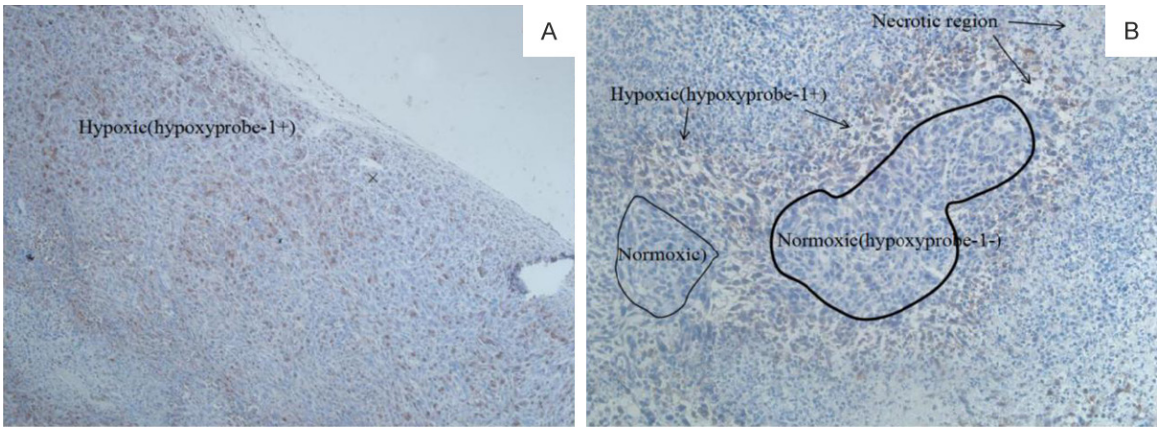

Figure S2. Immunohistochemical (IHC) staining with Hypoxyprobe-1 in a biopsy specimen of a primary tumor at day 14. (A) Original magnification is × 100; (B) Original magnification is × 200. White areas represent necrotic regions in which tumor cells have died from inadequate oxygen supply. The blue areas represent well-oxygenated (normoxic) cells, which are hypoxyprobe-1 negative. The brown staining indicates cells that are hypoxyprobe-1 positive, which are viable hypoxic cells.

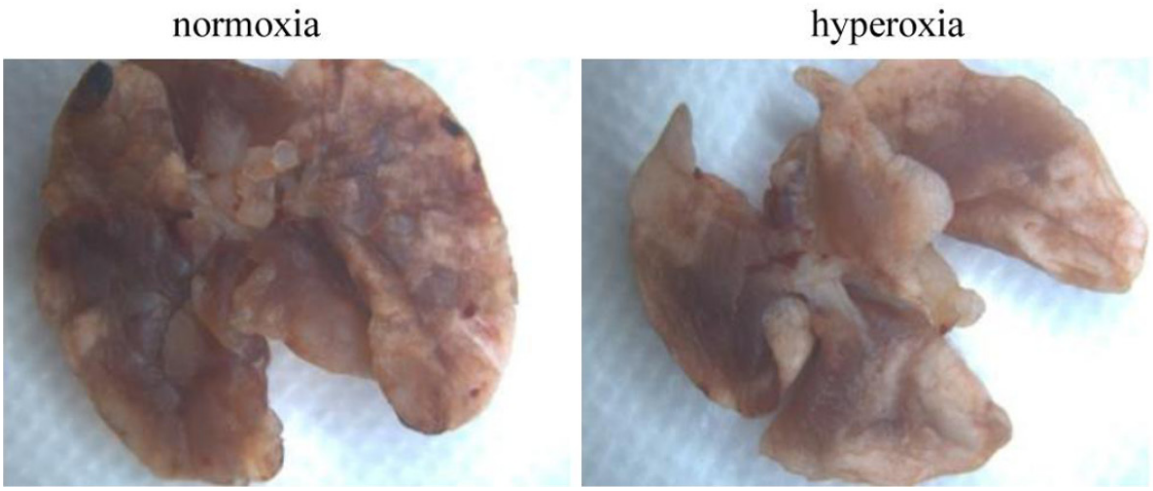

Figure S3. Respiratory hyperoxia inhibits lung metastasis formation in the 4T1 mammary carcinoma mouse model. Representative photographs of lungs with a high tumor burden harvested at day 28 from normoxia (left) and hyperoxia (right) treated groups of tumor bearing 4T1 mice.

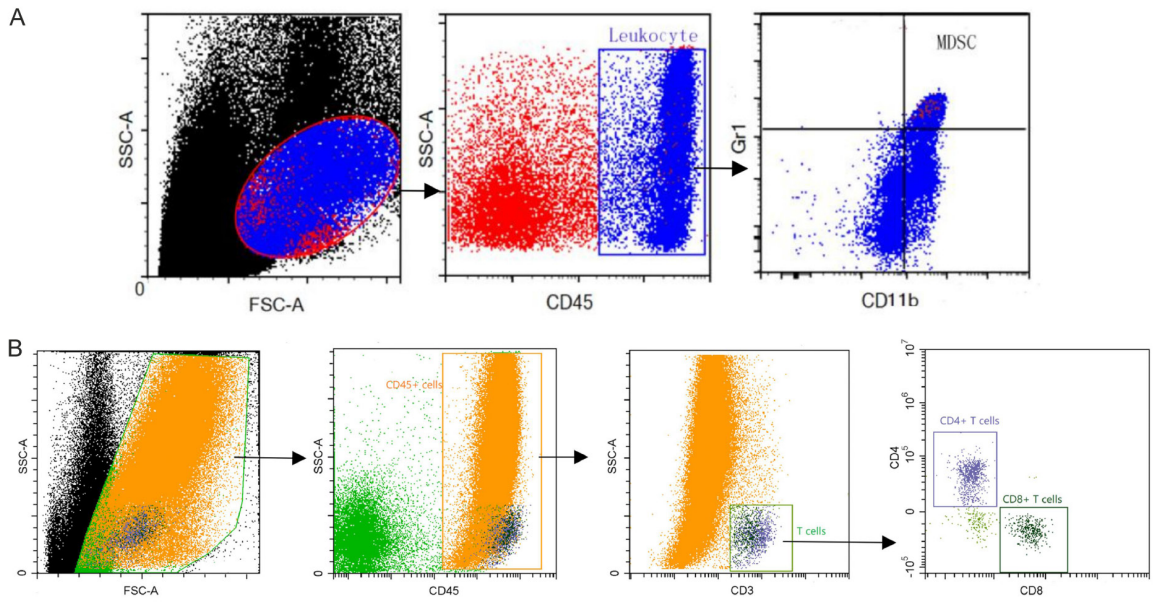

Figure S4. Fluorescence-activated cell sorting (FACS) analysis of MDSCs and T cells. Gating strategy and representative plots of (A) the MDSCs and (B) T-cell population.